A Spectral Method for 3D Shape Reconstruction and Denoising

A. Hero[1] and Jia Li[2]

1. Dept. EECS, Dept Biomedical Engineering, Dept Statistics
University of Michigan, Ann Arbor, MI

2. Dept ECE, Oakland University, Rochester, MI

http//www.eecs.umich.edu/~hero

Spherical Coordinate System

ϕ azimuth

θ elevation

$r(\theta, \phi)$

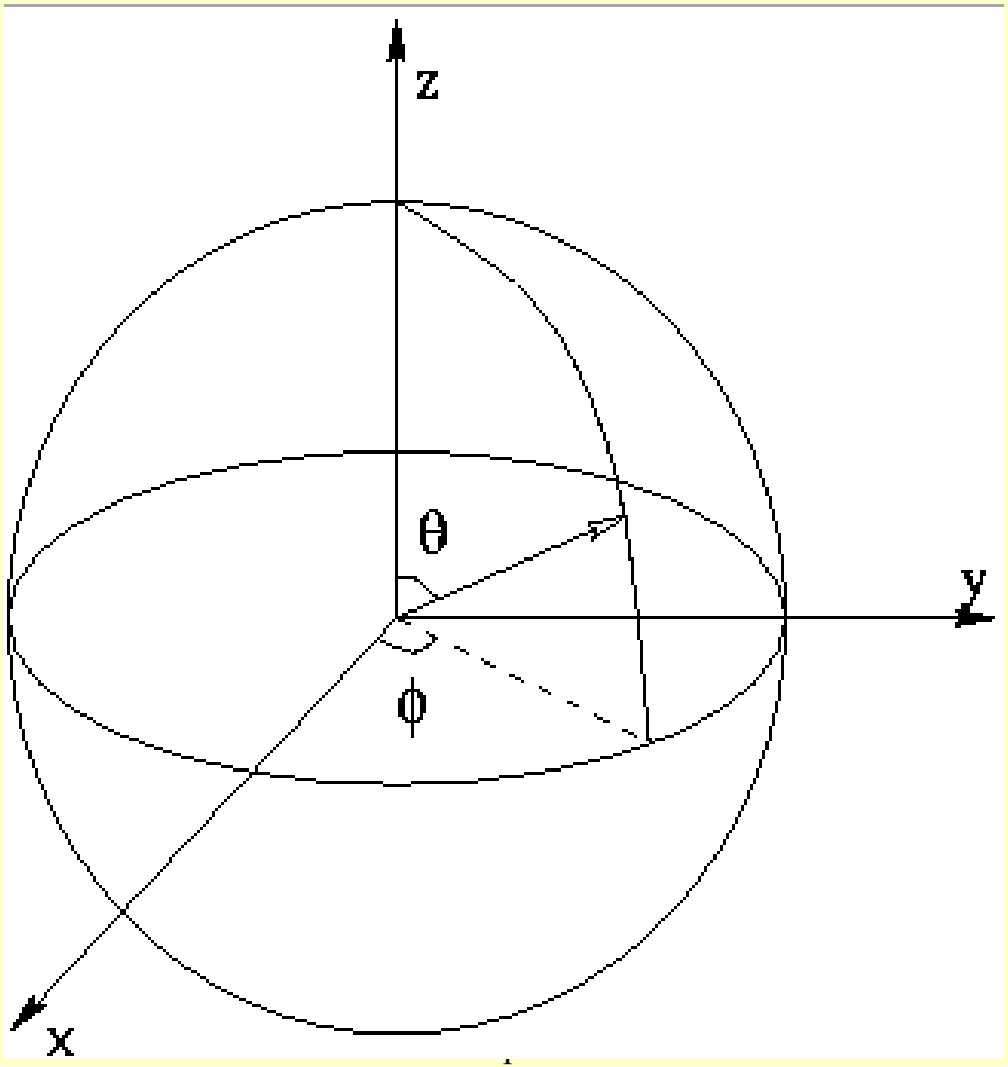

3D Fourier Descriptors

$$f(\theta,\phi) = \sum_{m=-\infty}^{\infty} f_m(\theta) e^{im\phi}$$

- Orthonormal basis
- Complete basis
- Ordered in increasing spatial frequency
- Common expansion in azimuth (longitude)

Spherical Harmonics

$$Y_l^m(\theta,\phi) = \underbrace{(-1)^m \sqrt{\frac{2l+1}{4\pi}\frac{(l-m)!}{(l+m)!}} P_l^m(\cos\theta)}_{f_{m,l}(\theta)} e^{im\phi}$$

- Angular solutions of Laplace equation on sphere
- Requires computation of Legendre polynomials
- Applied to shape approximation (Haigron&etal:98, Danielsson&etal:ICPR98, Matheny&etal:PAMI95)
- Implementation: SVD or FFT algorithm

First 10 Spherical Harmonics

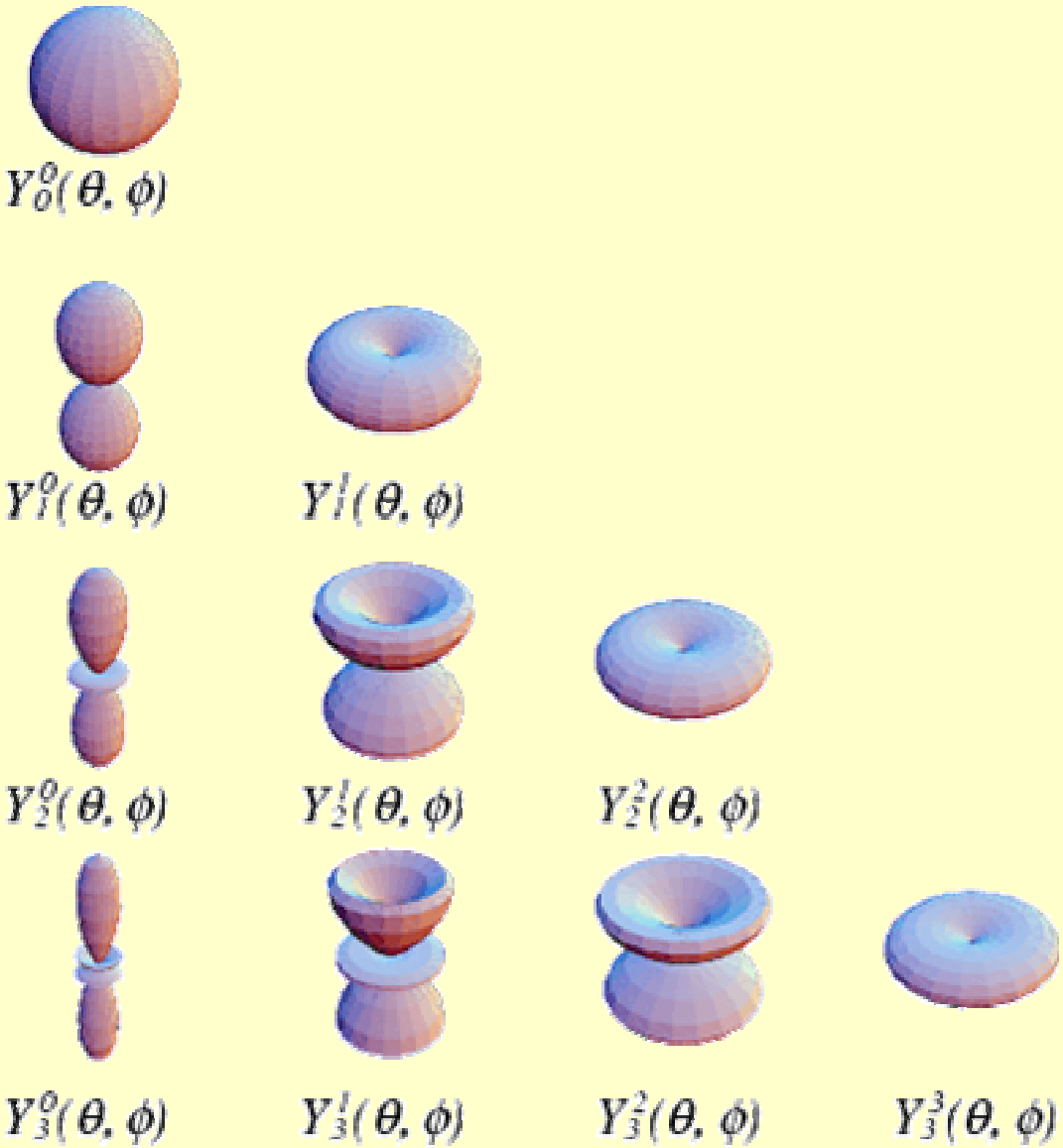

Computing Spherical Harmonic Coefficients

- SVD method via optimized sampling (Erturk&Dennis:ElectLett97, Matheny:PAMI95)
  $(K+1)^2$ unknown coefficients C

$$R(\theta,\phi) = \sum_{l=0}^{K} \sum_{m=-l}^{l} A_l^m U_l^m(\theta,\phi) + B_l^m V_l^m(\theta,\phi)$$

$$\mathbf{R} = \mathbf{UA} + \mathbf{VB} \Rightarrow \mathbf{R} = \mathbf{XC}$$

- Spherical FFT (Driscoll&etal:AdvAppMath94,Healy&etal:ICASSP96)
  - orthogonal discrete approximation to SH
  - lower complexity than SVD method
  - requires equi-spaced samples in azimuth/elevation

SH Numerical Comparisons

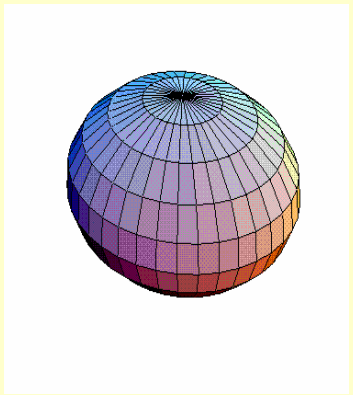

$$\left(\frac{x}{10}\right)^2+\left(\frac{y}{9}\right)^2+\left(\frac{z}{7}\right)^2=1$$

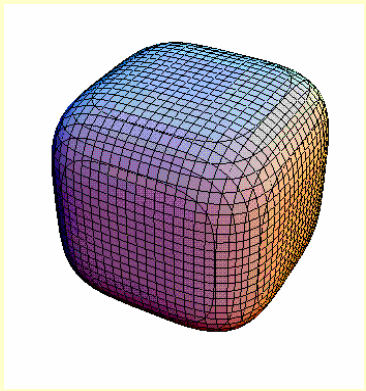

$$x^4+y^4+z^4=1$$

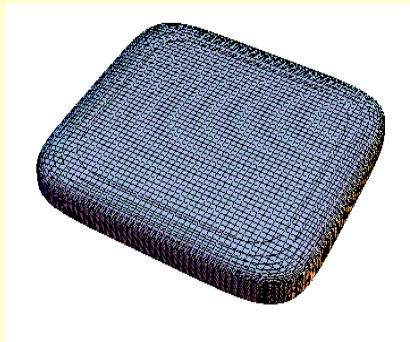

$$\left(\frac{x}{10}\right)^6+\left(\frac{y}{9}\right)^6+z^6=1$$

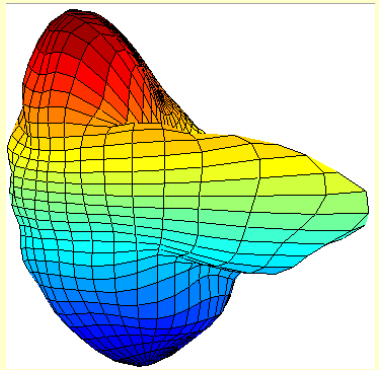

Liver Surface

3D Shapes used in the simulation

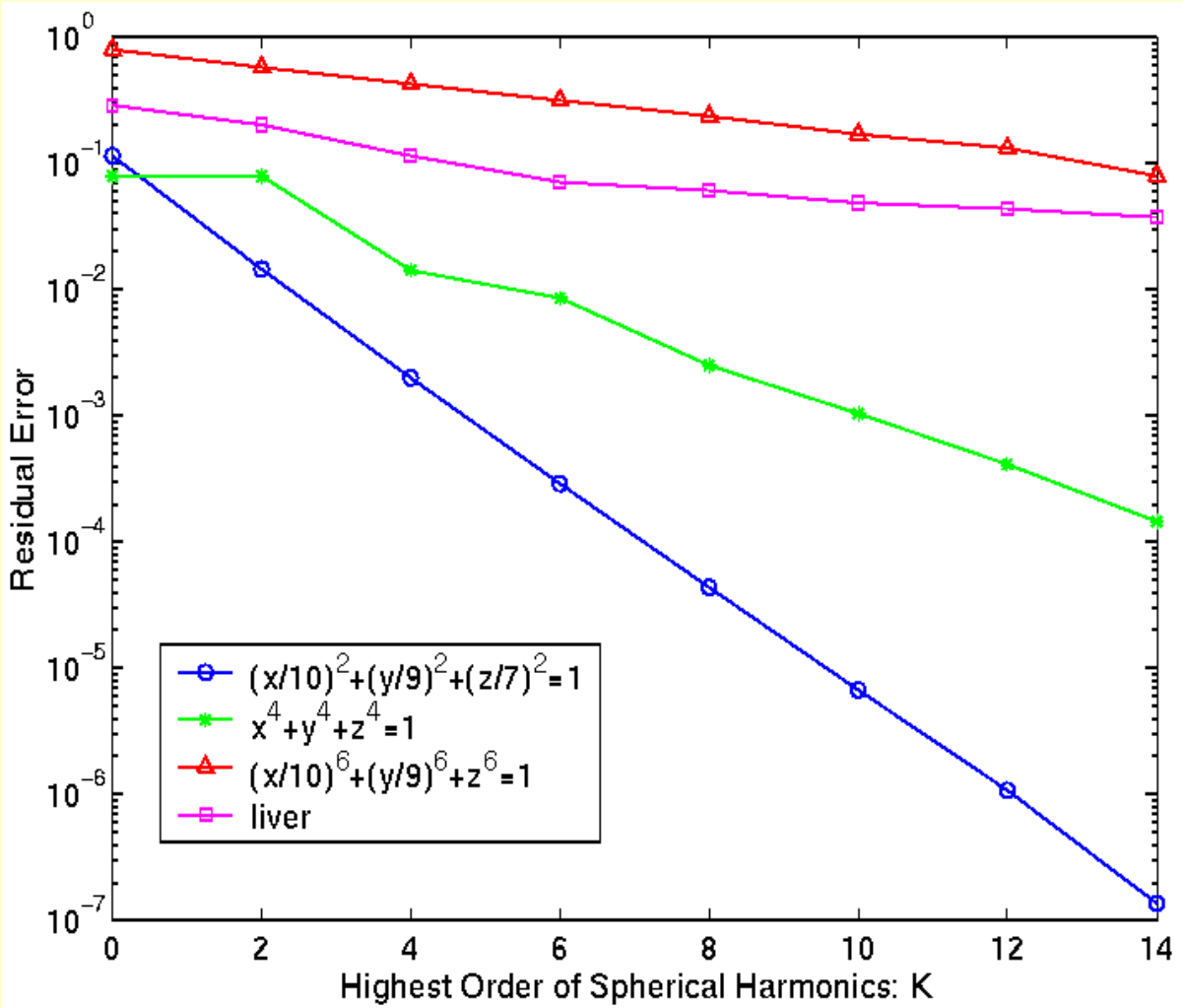

Shape modeling error vs. the highest order of spherical Harmonics for the four different shapes.

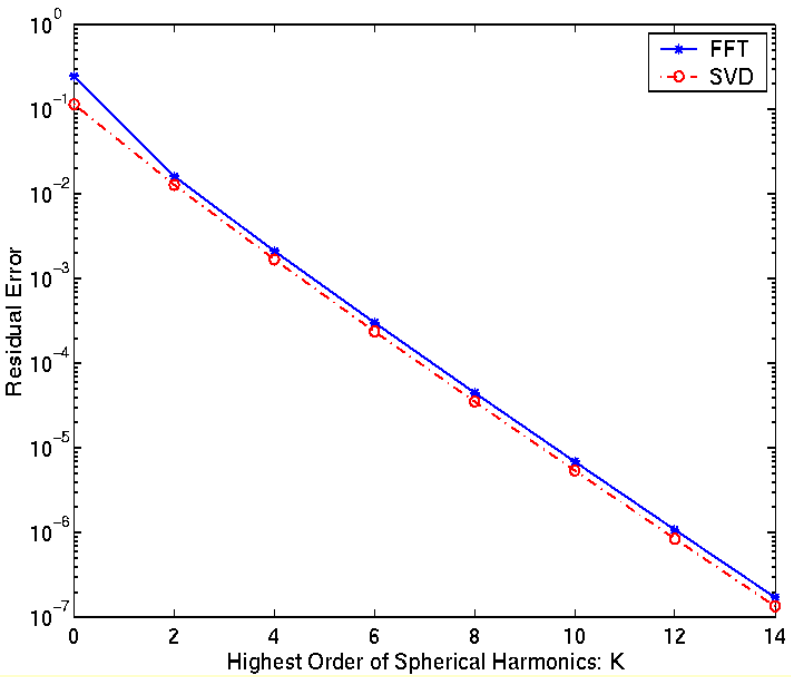

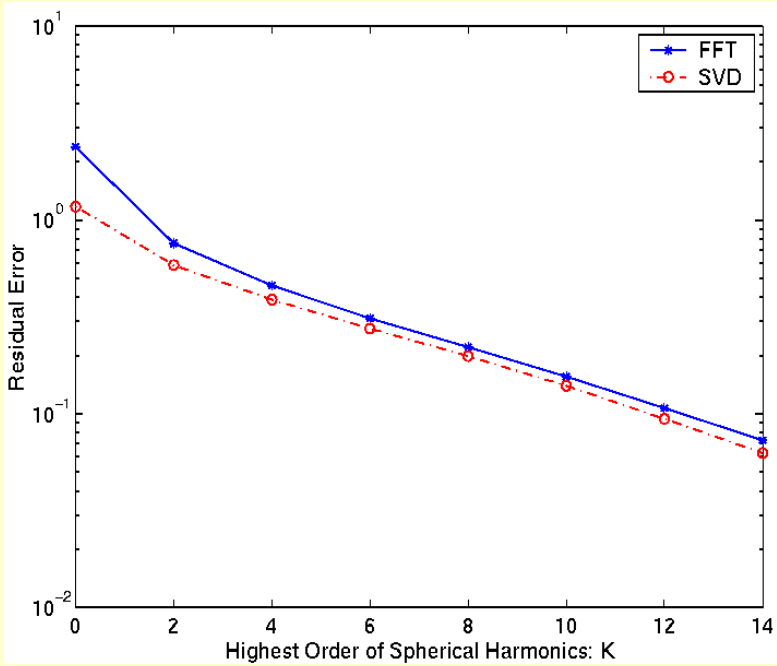

$$(\frac{x}{10})^2+(\frac{y}{9})^2+(\frac{z}{7})^2=1$$

$$(\frac{x}{10})^6+(\frac{y}{9})^6+z^6=1$$

The shape modeling errors vs. the highest degree of spherical harmonics by the FFT algorithm and the SVD algorithm.

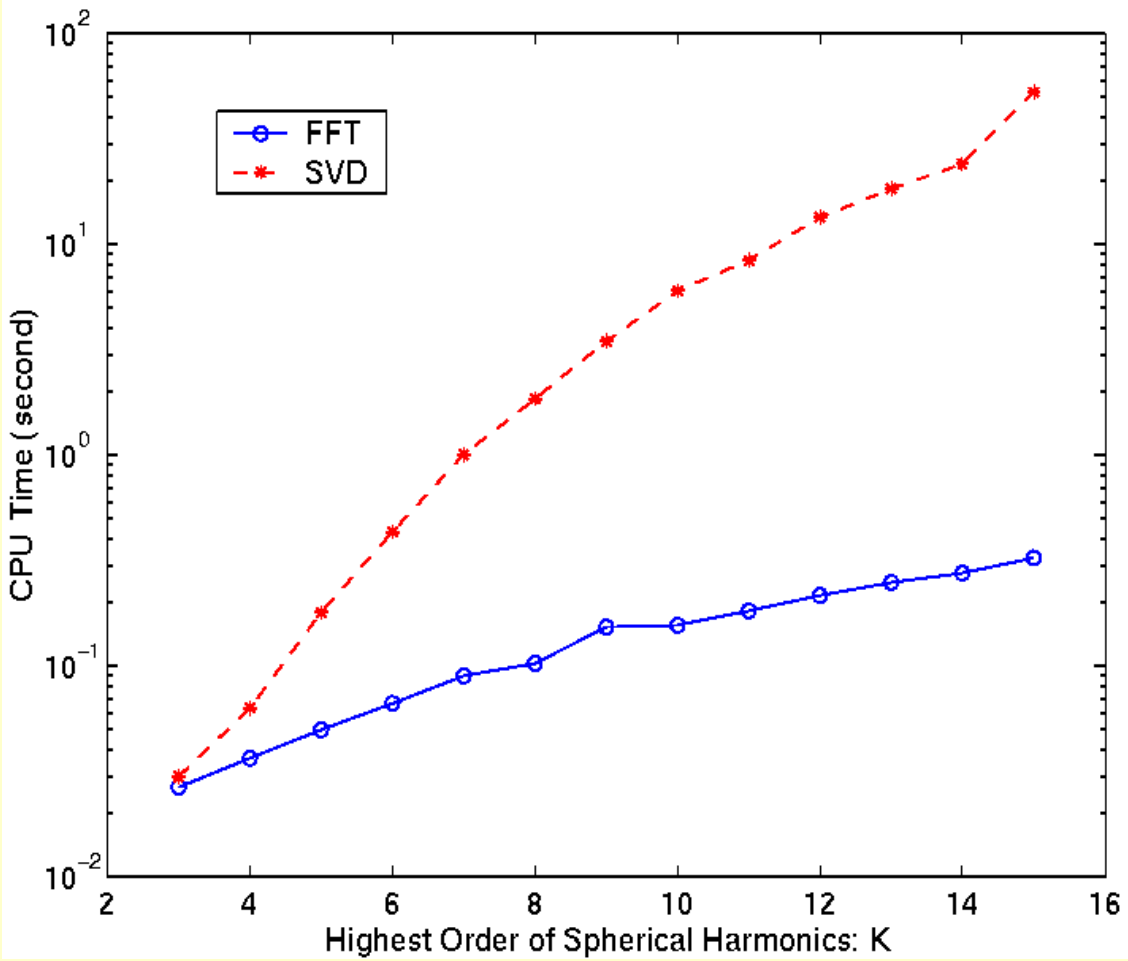

CPU time comparison between the SVD and FFT algorithms

Double Fourier Series

- DFS are easier to manipulate than SH
- DFS over the sphere is more difficult than over R^2
- Boundary conditions for $f_m(\theta)$ at spherical poles

$$f_m(\theta) = \begin{cases} finite, & m = 0 \\ 0, & m \neq 0 \end{cases}$$

$$\frac{d}{d\theta} f_m(\theta) = \begin{cases} finite, & \text{odd} \quad m \\ 0, & \text{even} \quad m \end{cases}$$

- Standard 2D trigonometric series not admissible!
- Are there interesting admissible bases besides SH?

Admissible DFS Expansion

$$f_m(\theta) = \sum_{n=0}^{J-1} f_{n,0} \cos n\theta, \quad m = 0$$

$$f_m(\theta) = \sum_{n=1}^{J} f_{n,m} \sin n\theta, \quad \text{odd } m,$$

$$f_m(\theta) = \sum_{n=1}^{J} f_{n,m} \sin\theta \sin n\theta, \quad \text{even } m \neq 0.$$

Fourier coefficients can be computed using fast sin and cos transform

(Ref: Cheong:JournCompPhysics00)

Decomposition of Isotropic Random Fields Over Unit Sphere Using SH

- Isotropic field satisfies

$$E\left\{X(\theta_1,\phi_1)X^*(\theta_2,\phi_2)\right\} = R(\gamma) = \psi(\cos\gamma)$$

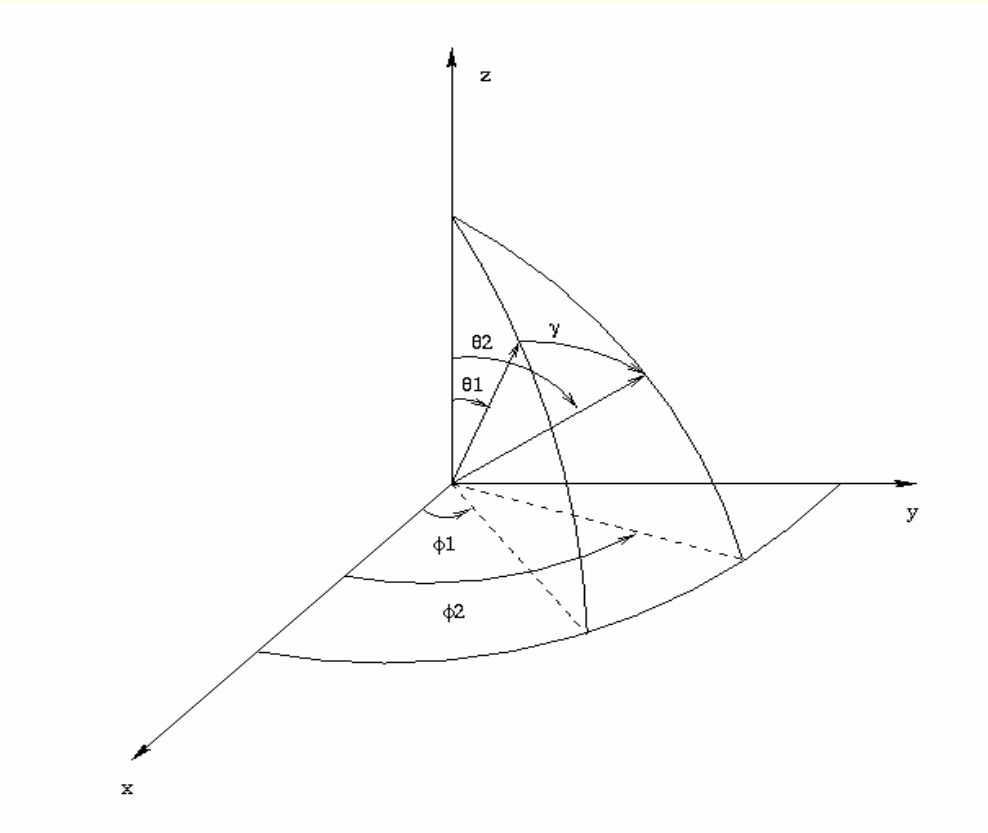

Isotropic Random Field Model

– Theorem: Let $f(x): S^2 \rightarrow R$ be the radial function of a polar object which center has been aligned with origin. If the object center is fixed at origin and the orientation of the object is uniformly distributed, the observed radial function F(x) is a sample from an isotropic random field over the unit sphere.

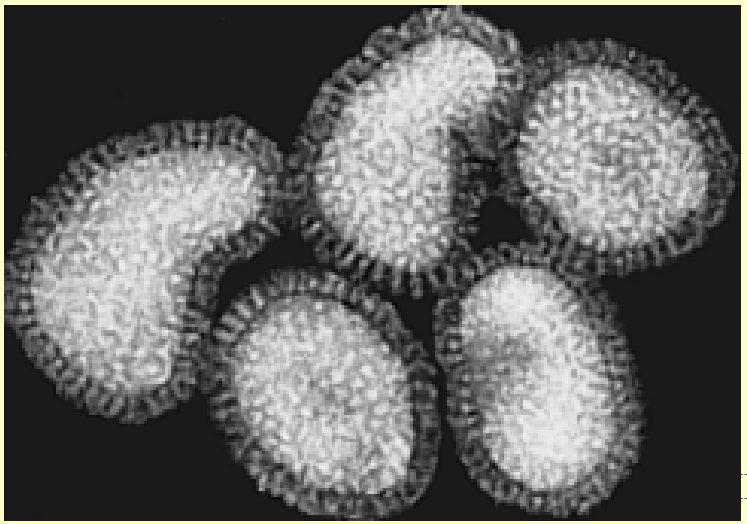

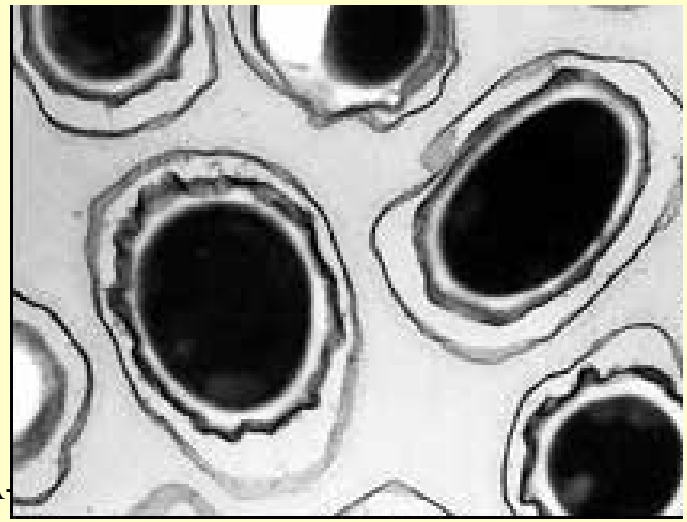

Karhunen-Loeve Expansion

SH are eigenfunctions of isotropic r.f. on sphere (Yadrenko:76)

$$X(\theta,\phi) = \sum_{l=0}^{\infty} \sum_{m=-l}^{l} A(l,m) Y_l^m(\theta,\phi)$$

$$A(l,m) = \int_{S^2} X(\theta,\phi) Y_l^{m*}(\theta,\phi) d\Omega$$

$$E\{A(l,m)\} = 0$$

$$E\{A(l,m) A^*(l',m')\} = \lambda_l \delta_{l,l'} \delta_{m,m'}$$

$$\lambda_l = 2\pi \int_{-1}^{1} \psi(t) P_l(t) \mathrm{d}t$$

Registration/Reconstruction

- Rotation $g \in SO(3)$
- Euler angles (α, β, γ)
- SH representations:

$$R(\theta,\phi) = \sum_{l=0}^{K} \sum_{m=-l}^{l} c_l^m Y_l^m(\theta,\phi) \qquad \text{(reference)}$$

$$\tilde{R}(\theta,\phi) = \sum_{l=0}^{K} \sum_{m=-l}^{l} \tilde{c}_l^m Y_l^m(\theta,\phi) \qquad \text{(rotated reference)}$$

$$\tilde{c}_l^m = \sum_{m'=-l}^{l} D^l_{mm'}(\alpha,\beta,\gamma) c_l^{m'}$$

$$D^l_{mm'}(\alpha,\beta,\gamma) = \exp(-im\alpha) \cdot d^l_{mm'}(\beta) \cdot \exp(-im'\gamma)$$

SH and Transformations Over SO(3)

Linear SH domain representation of spatial rotation (Wigner:59)

$$\begin{pmatrix} \tilde{c}_0^0 \\ \tilde{c}_1^{-1} \\ \tilde{c}_1^0 \\ \tilde{c}_1^1 \\ \tilde{c}_2^{-2} \\ \tilde{c}_2^{-1} \\ \tilde{c}_2^0 \\ \tilde{c}_2^1 \\ \tilde{c}_2^2 \\ \vdots \end{pmatrix} = \begin{pmatrix} D^{(0)} & & & \\ & \begin{pmatrix} & & \\ & D^{(1)} & \\ & & \end{pmatrix} & & \\ & & \begin{pmatrix} & & \\ & D^{(2)} & \\ & & \end{pmatrix} & \\ & & & \ddots \end{pmatrix} \begin{pmatrix} c_0^0 \\ c_1^{-1} \\ c_1^0 \\ c_1^1 \\ c_2^{-2} \\ c_2^{-1} \\ c_2^0 \\ c_2^1 \\ c_2^2 \\ \vdots \end{pmatrix}$$

Joint Registration of 3D Rotation and Spherical Harmonic Coefficients

- Gaussian model

$$c_l^m = a_l^m + \eta_l^m$$

$$\tilde{c}_l^m = \sum_{n=-l}^{l} D_{mn}^l(\alpha,\beta,\gamma) a_l^n + \tilde{\eta}_l^m$$

- Marginal coefficient likelihood functions

$$L_{c_l^m} = \exp\left(-(c_l^m - a_l^m)^2 / 2\sigma_l^2\right)$$

$$L_{\tilde{c}_l^m} = \exp\left(-(\tilde{c}_l^m - \sum_{n=-l}^{l} D_{mn}^l(\alpha,\beta,\gamma) a_l^n)^2 / 2\tilde{\sigma}_l^2\right)$$

- ML estimator:

$$\{\hat{\alpha},\hat{\beta},\hat{\gamma},\{\hat{a}_l^m\}\} = \underset{\alpha,\beta,\gamma,\{a_l^m\}}{\operatorname{argmin}} \sum_{l=1}^{K}\sum_{m=-l}^{l}\left(\frac{(c_l^m - a_l^m)^2}{\sigma_l^2} + \frac{(\tilde{c}_l^m - \sum_{n=-l}^{l} D_{mn}^l(\alpha,\beta,\gamma) a_l^n)^2}{\tilde{\sigma}_l^2}\right)$$

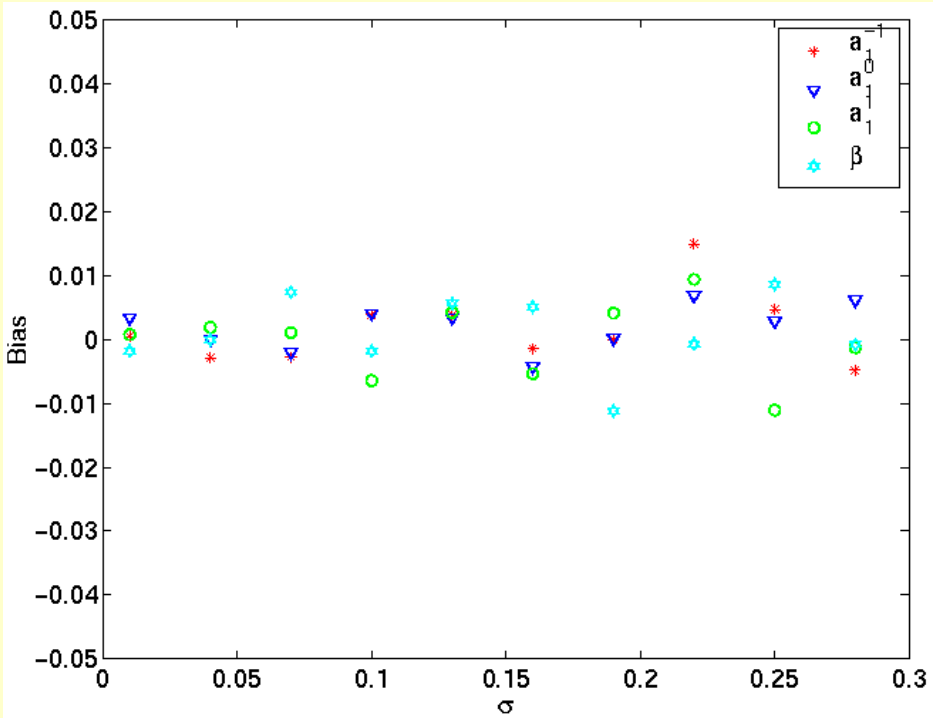

Bias

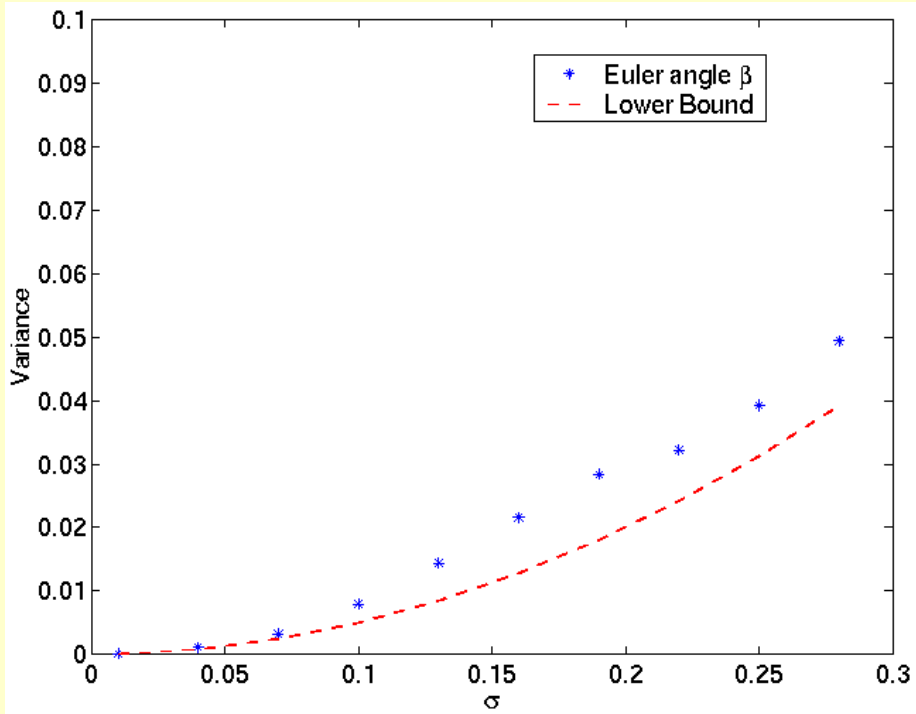

Variance and CR bound

The performance of the maximum likelihood estimator which jointly estimates the Euler angles and the shape parameters.

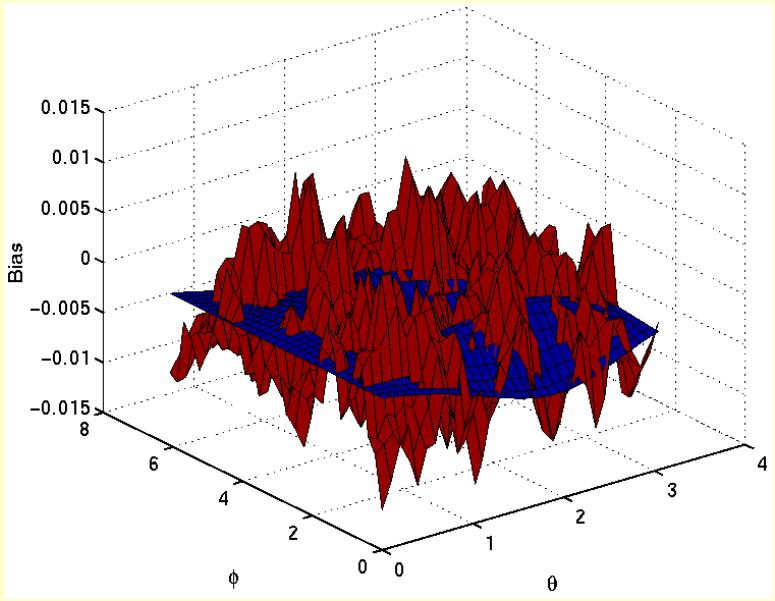

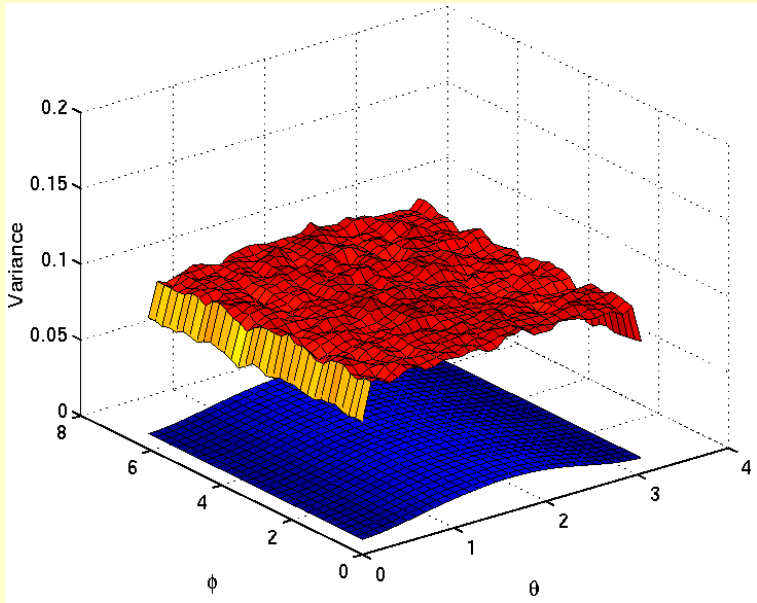

Bias and variance of radial reconstruction For Lowpass(red) and Wiener(blue) filter

3D Center Estimation

- Quadratic surface

$$Ax^2 + By^2 + Cz^2 + Dxy + Exz + Fyz + Gx + Hy + Iz + J = 0$$

- Segmented surface data $\{(x_i, y_i, z_i), i = 1 \cdots N\}$
- Estimator (Bookstein:CGIP77)

$$(\hat{A}, \hat{B}, \cdots \hat{J}) = \arg\min_{(A,B,\cdots J)} \sum_i Q^2(x_i, y_i, z_i)$$

- Error function

$$Q(x_i, y_i, z_i) = Ax_i^2 + By_i^2 + Cz_i^2 + Dx_i y_i + Ex_i z_i + Fy_i z_i + Gx_i + Hy_i + Iz_i + J$$

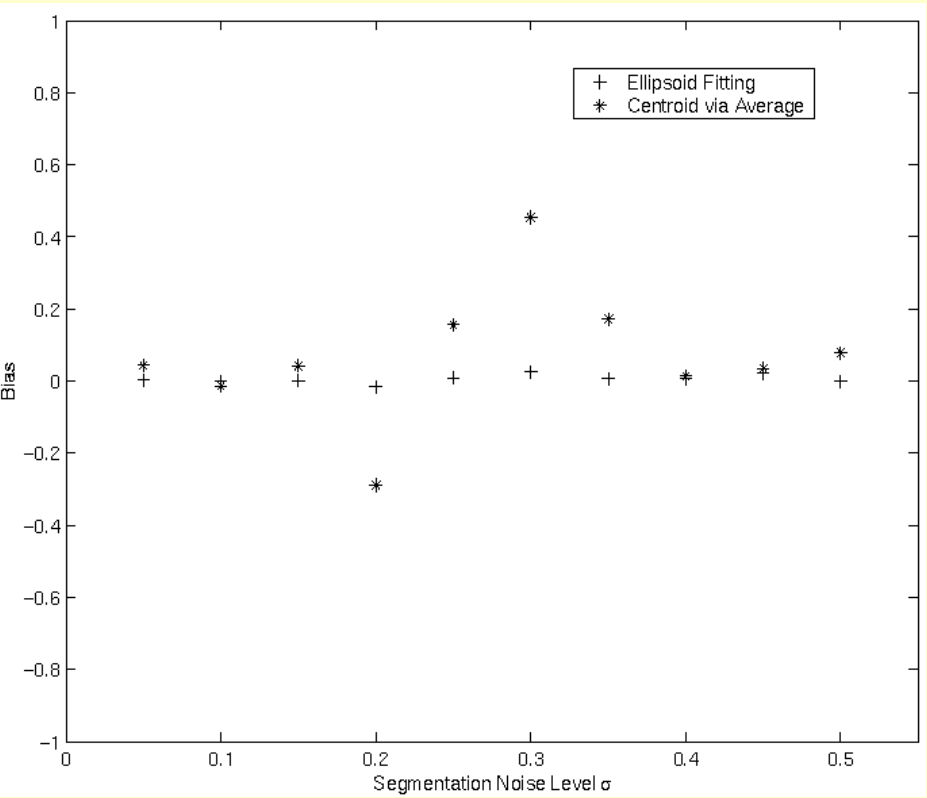

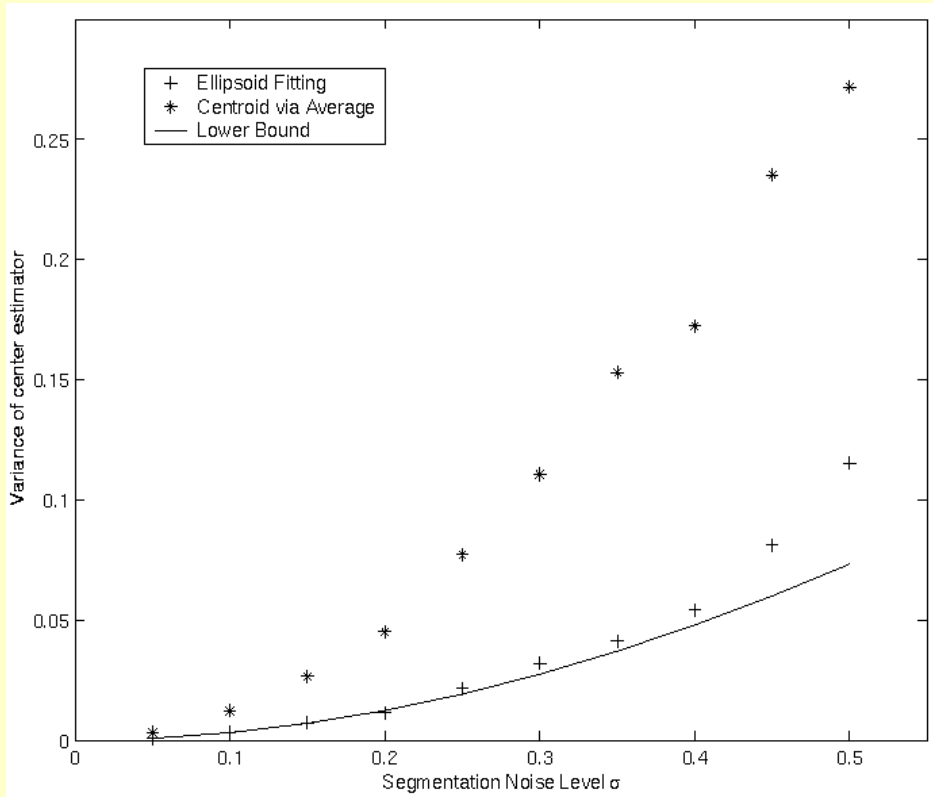

Comparison between averaging center estimator and ellipsoid center estimator.

Application: Surface Segmentation and Reconstruction

- Edge detection and thresholding
- ML/MAP/LS methods of shape recovery
  - Spline models (Hero&etal:IT99)
  - MRF (Zhang&etal:MI01)
- Deformable models (active contours) of shape recovery: "front propagation"
  - Parametric "snakes" and balloons (Cohen&Cohen:PAMI93,Kass&etal:IJCV87)
  - Geometric "level sets" (Casselles&etal:NumerMath93, Malladi&etal:PAMI95)

Application to Active Contour Surface Reconstruction

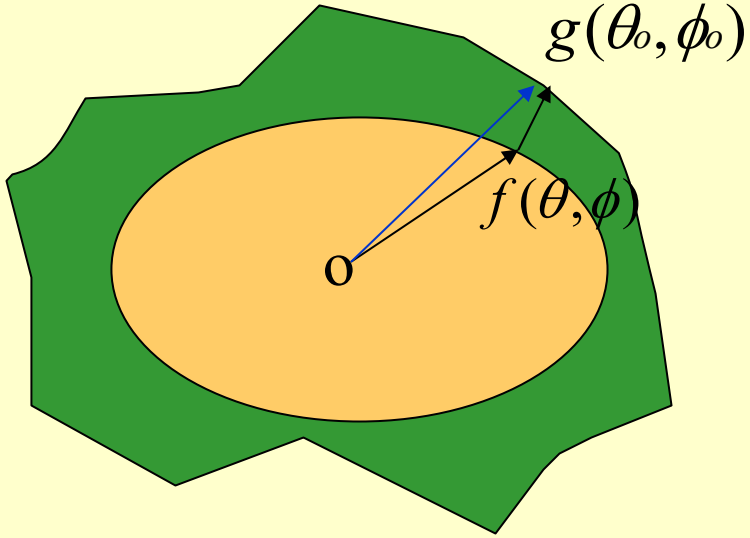

$$E(f) = \int_{S^2} ((f - g_f)^2 + \alpha \left\| \nabla f \right\|^2) d\Omega$$

$\alpha = 1/\mu$: non-negative smoothness parameter

Polar Euler-Lagrange Equation

Minimizer f of E(f) must satisfy PDE over S^2

$$\nabla^2 f - \mu(f - g_f)(1 - \frac{\partial g_f}{\partial f}) = 0$$

$$\nabla^2 = \frac{1}{\sin\theta}\frac{\partial}{\partial\theta}(\sin\theta\frac{\partial}{\partial\theta}) + \frac{1}{\sin^2\theta}\frac{\partial^2}{\partial\phi^2}$$

Front propagation consists of two steps:

1.Update f: (solve Helmholtz)

$$(1/\mu)\nabla^2 f_{n+1} - f_{n+1} = -(f_n - g_{f_n})\frac{\partial g_{f_n}}{\partial f_n} - g_{f_n}$$

2.Update g: (compute boundary attraction map)

$$g_{f_n} \rightarrow g_{f_{n+1}}$$

Methods of Solving Helmholtz

$$\nabla^2 f - \mu(f - g) = 0$$

- Iterative FEM and FDM
  - Advantage: non-uniform sampling can be accommodated
  - Disadvantage: very high computational complexity
- Non-iterative spectral methods
  - Spherical harmonic expansions
  - Double Fourier series

Comparison:

- Grid size $N \times N$
- Computational complexity
  - FEM/FDM Method $O(N^6) \sim O(N^3)$
  - Spectral Method $O(N^2 \log N)$

Spectral Methods for Elliptic Equations on Unit Sphere

- Weather modeling and prediction
  - –Boer&etal:Atmosphere75,Boyd:WeatherRev78
- Ocean dynamics modeling
  - –Voigt&etal:SIAM84
- Accelerations:
  - DFS: Yee:WeatherRev81,Cheong:JCompPhysics00

Spectral Solution to Helmholtz

$$f(\theta,\phi) = \sum_{m=-\infty}^{\infty} f_m(\theta) e^{im\phi}$$

Fourier Descriptor

$$f_m(\theta) = \sum_{n=-\infty}^{\infty} f_{m,n} \cos(\, n\theta + n\pi/2\,)$$

Cheong's trig series

1. Substitute Fourier descriptor $f_m(\theta)$ into Helmholtz equation

$$\frac{1}{\sin\theta}\frac{d}{d\theta}(\sin\theta\frac{d}{d\theta}f_m(\theta)) - \frac{m^2}{\sin^2\theta}f_m(\theta) = \mu\left[f_m(\theta) - g_m(\theta)\right]$$

2. Substitute Cheong's expansion of $f_m(\theta)$

Helmholtz Recursions

$$\frac{(n-1)(n-2)+\mu}{4} f_{n-2,m} - \frac{n^2+2m^2+\mu}{2} f_{n,m} + \frac{(n+1)(n+2)+\mu}{4} f_{n+2,m}$$

$$= \mu\left(\frac{1}{4} g_{n-2,m} - \frac{1}{2} g_{n,m} + \frac{1}{4} g_{n+2,m}\right) \qquad m = 0, \text{ or odd}$$

$$\frac{n(n-1)+\mu}{4} f_{n-2,m} - \frac{n^2+2m^2+\mu}{2} f_{n,m} + \frac{n(n+1)+\mu}{4} f_{n+2,m}$$

$$= \mu\left(\frac{1}{4} g_{n-2,m} - \frac{1}{2} g_{n,m} + \frac{1}{4} g_{n+2,m}\right) \qquad m \text{ even and} \neq 0$$

After truncation obtain tridiagonal linear system

$$B\mathbf{f} = A\mathbf{g}$$

$$\begin{pmatrix} b_{1,m} & c_1 & & & & \\ a_3 & b_{3,m} & c_3 & & & \\ & \ddots & \ddots & \ddots & & \\ & & a_{J-3} & b_{J-3,m} & c_{J-3} & \\ & & & a_{J-1} & b_{J-1,m} & \end{pmatrix} \begin{pmatrix} f_{1,m} \\ f_{3,m} \\ \vdots \\ f_{J-3,m} \\ f_{J-1,m} \end{pmatrix} = \begin{pmatrix} 2 & -1 & & & & \\ -1 & 2 & -1 & & & \\ & \ddots & \ddots & \ddots & & \\ & & -1 & 2 & -1 & \\ & & & -1 & 2 & \end{pmatrix} \begin{pmatrix} g_{1,m} \\ g_{3,m} \\ \vdots \\ g_{J-3,m} \\ g_{J-1,m} \end{pmatrix}$$

1. $g(\theta,\phi) \rightarrow g_{n,m}$
2. Obtain $f_{n,m}$ by solving matrix equations
3. $f_{n,m} \rightarrow f(\theta,\phi)$

Experiment 1: Ellipsoidal Surface Reconstruction Different Regularization Parameters

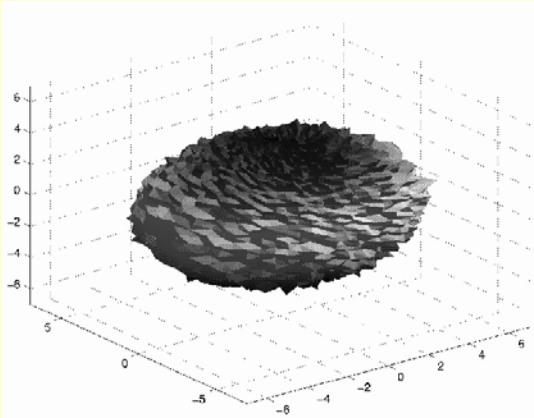

Original segmentation

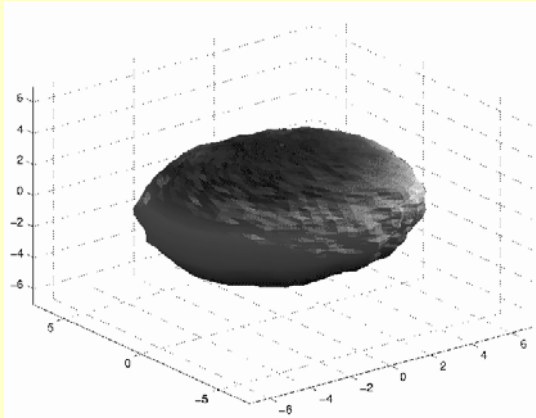

$\mu = 10^4$

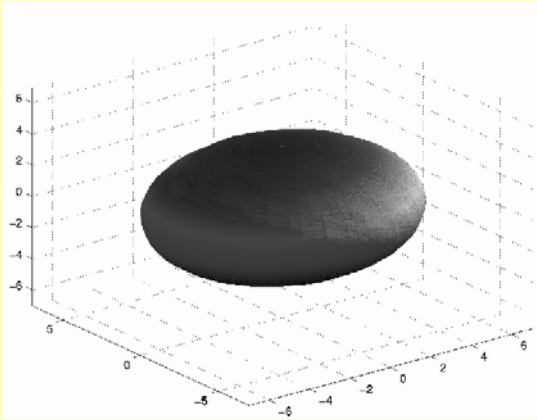

$\mu = 10^3$

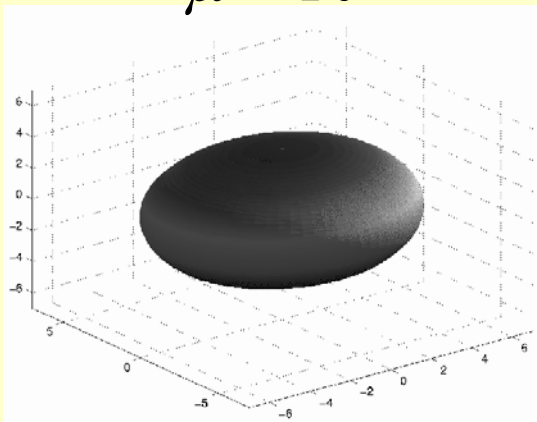

$\mu = 10^2$

Data Regularization Parameter

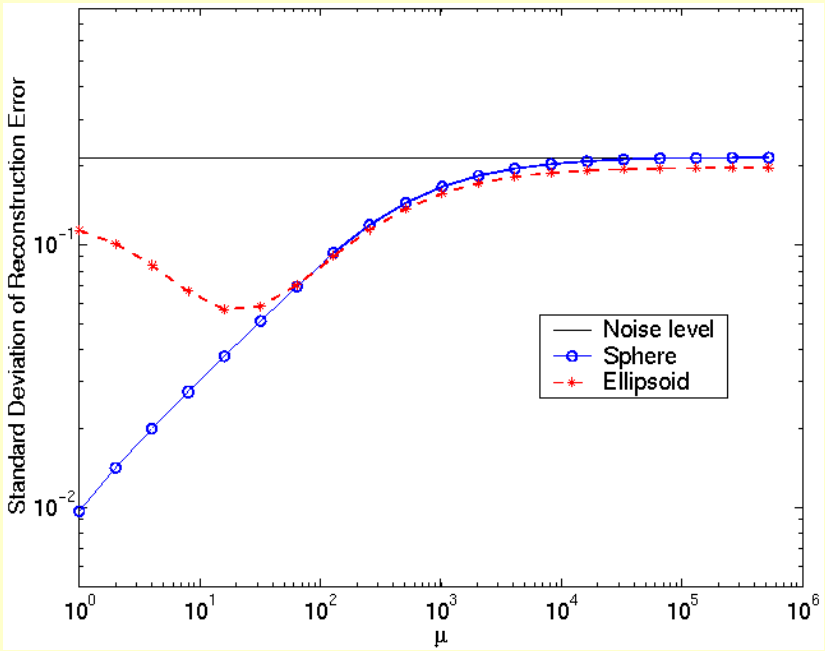

Different shapes

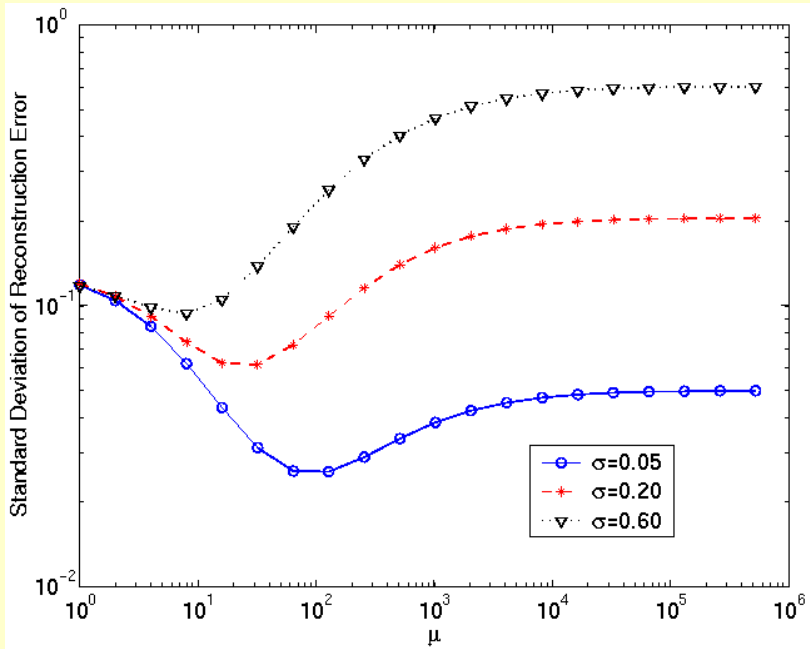

Different noise levels

Experiment 2: CT Thoracic Slices

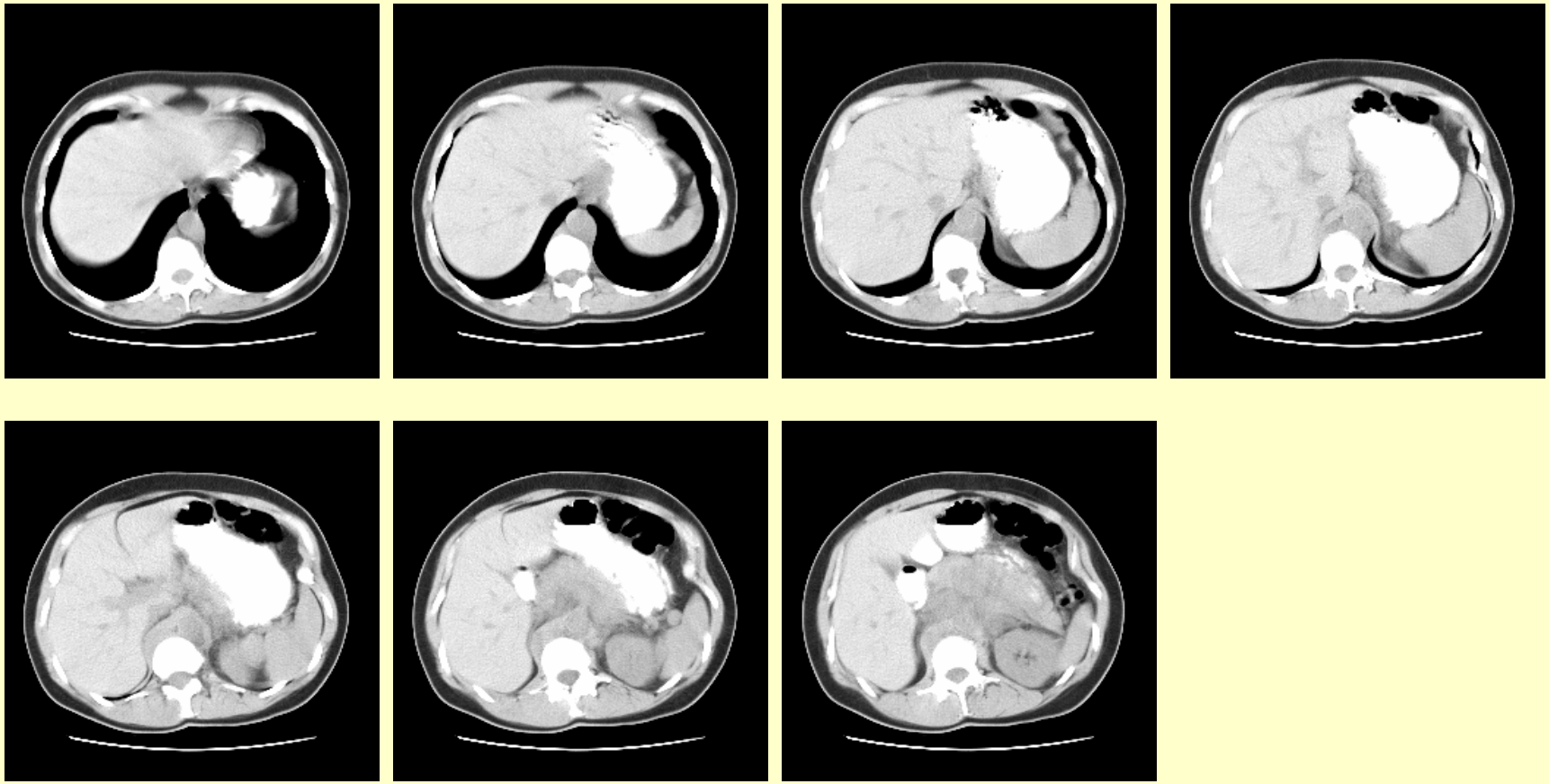

Edge-maps

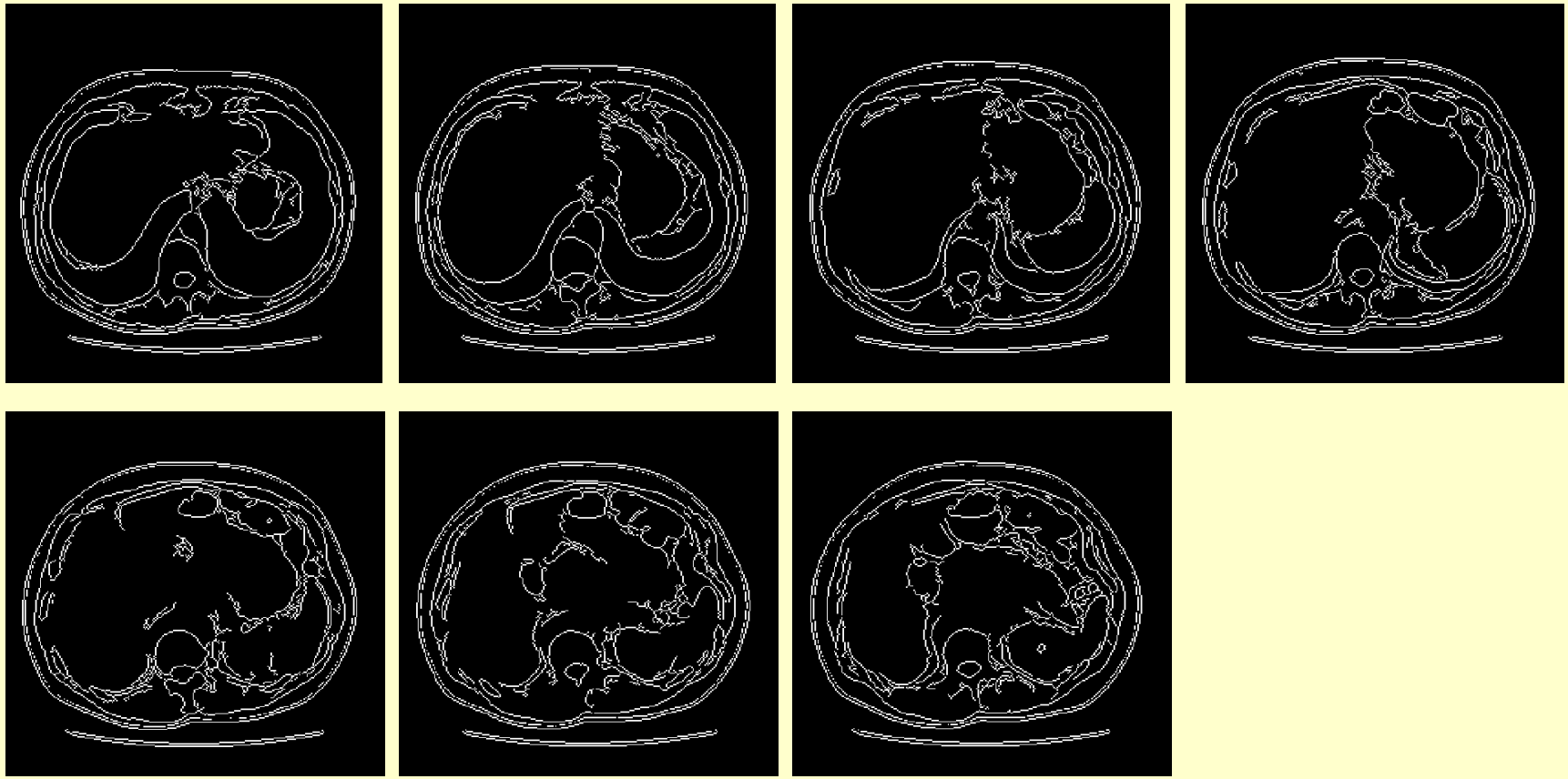

Active Contour Implementation

- Liver center estimated via ellipsoid fitting
- Local edge detection gives coarse segmentation
- 32 x 32 angular grid used for radial descriptor
- Elliptic evolving contour computed via spectral method
- Convergent to within a pixel after 5 iterations
- 3 values of μ investigated:

$$\mu = 10^3, \mu = 10^4, \mu = 10^6$$

Segmentation After 5 Iterations

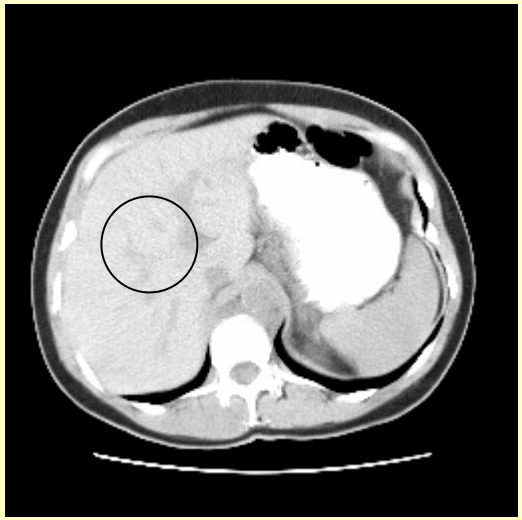

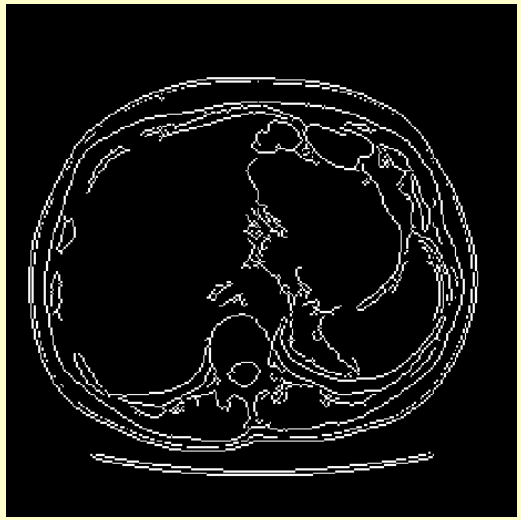

$\mu = 10^3$

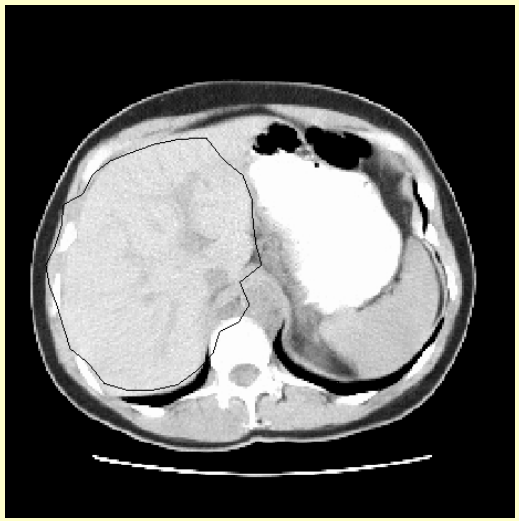

$\mu = 10^4$

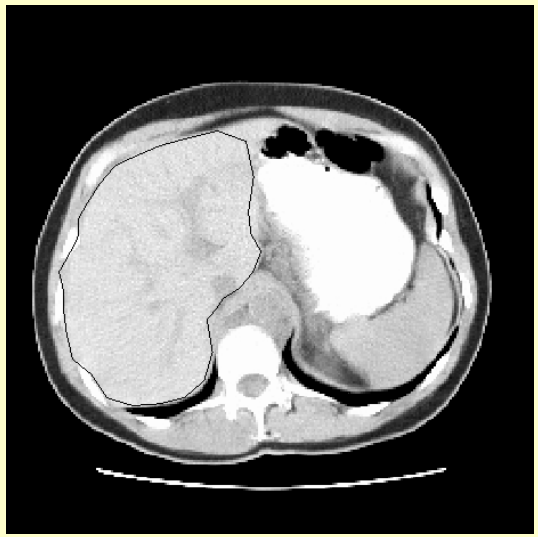

$\mu = 10^6$

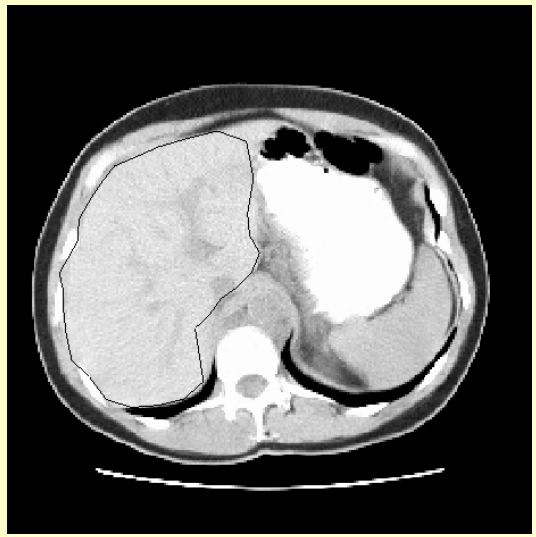

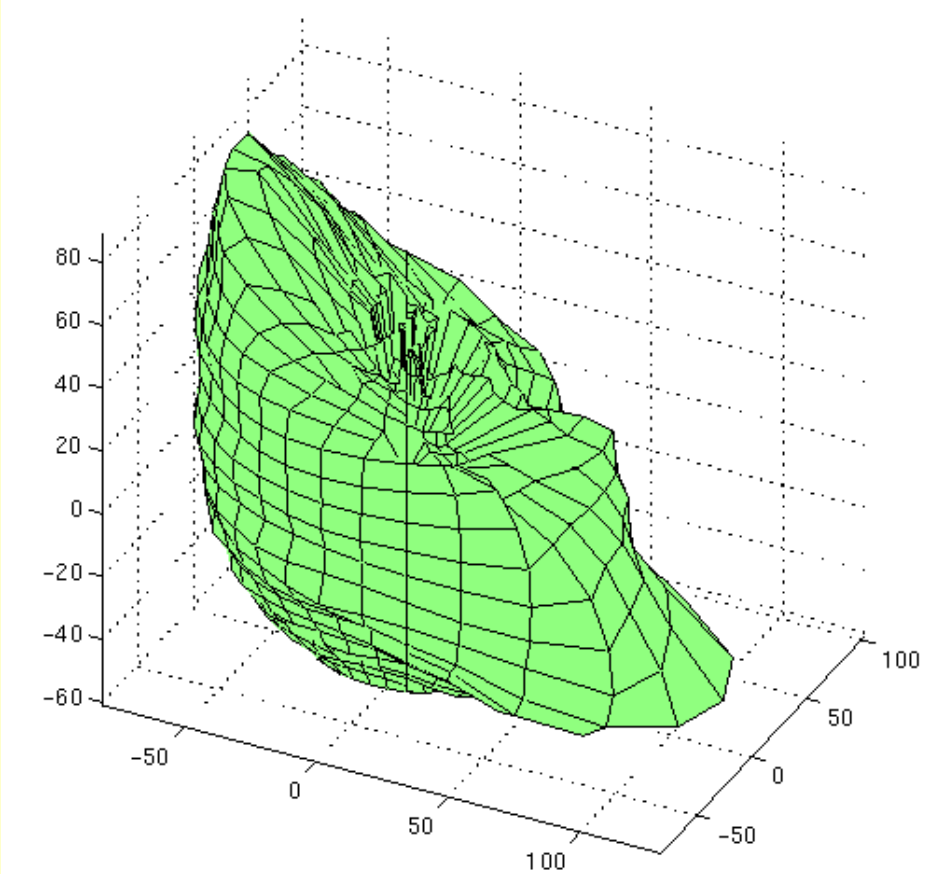

No regularization

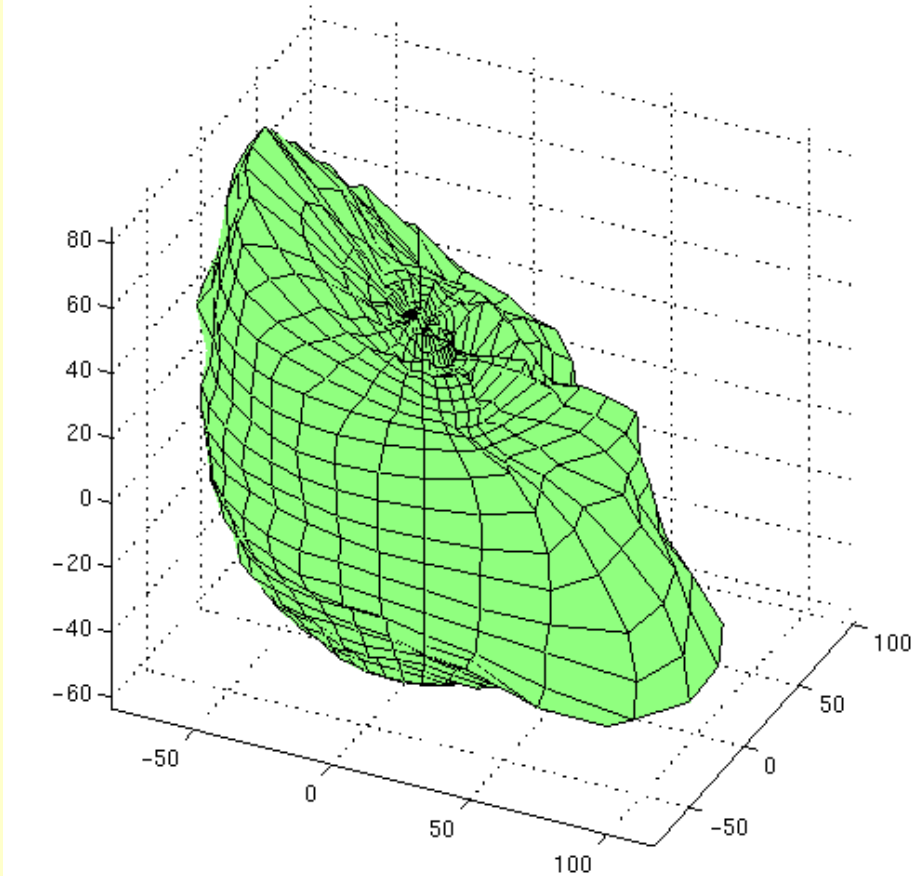

$\mu = 10^4$

Reconstruction of liver surface from 2D CT slices

Conclusions

- SH lead to optimal shape filtering and ML registration of polar 3D objects having isotropic random field models
- DFS/SH lead to spectral method for Helmholtz PDE introduced for 3D active balloons
- Application of recent advances in computational fluid dynamics to shape recovery problem
- Accelerated performance of parametric active contour on real and synthetic 3D images